GPS Solutions (2025) 29:33
https://doi.org/10.1007/s10291-024-01793-6

ORIGINAL ARTICLE

The 2024 GPS accuracy improvement initiative

O. Montenbruck[1] · **P. Steigenberger**[1]

Received: 4 October 2024 / Accepted: 23 November 2024

Abstract
Following several performance enhancements, GPS has provided a stable signal-in-space range error (SISRE) of about 50 cm (RMS) for more than a decade. As of early 2024, a major SISRE reduction by about 30% could be noted that helps to maintain the competitiveness of GPS in comparison with the Chinese BeiDou system and reduces the performance difference with respect to the European Galileo system. Based on analyses of onboard clock stability and broadcast navigation messages, the SISRE enhancement can be attributed to a combination of clock switches on selected satellites as well as an overall reduction of the mean time between navigation data uploads. The additional adoption of new transmit antenna phase center offsets in the control segment has no immediate performance impact but affects the comparison of broadcast and precise orbits. Following the aforementioned operational changes, SISRE values for dual-frequency P(Y)-code positioning with the legacy navigation message (LNAV) were found to decrease to roughly 30 cm from March 2024 onward, and marginally worse results are obtained for users of the civil L1/L2 signals and the L2 civil navigation (CNAV) message. Single-frequency LNAV users, on the other hand, experience only a minor benefit, since orbit and clock information improvements are largely masked by the non-availability of group delay information for the L1 C/A signal relative to the L1 P(Y) signal.

Keywords SISRE · GPS · Broadcast Ephemeris · Clocks · Upload Interval

Introduction

The concept of signal-in-space range error (SISRE) monitoring was introduced by Bernstein (1983) as a means for assessing the GPS service performance. The SISRE describes the joint effect of orbit, clock, and group delay errors on the modeled pseudorange in single-point positioning (SPP). It aggregates the contributions of the control and space segment to the achievable positioning performance, and separates them from the user equipment errors (UEEs) which comprise, for example, receiver noise and multipath, but also unmodelled atmospheric path delays (Langley et al. 2017).

A generic framework for SISRE analysis based on the comparison of broadcast orbits, clocks, and signal-specific group delays (described by subscript "bce") and precise products (denoted by subscript "ref") has previously been presented in Montenbruck et al. (2018). For proper comparison, satellite positions $\boldsymbol{r}^s$ and clock offsets cdt^s of broadcast and precise ephemerides are jointly transformed to the center of mass (CoM) as a common reference point using the corresponding antenna offsets. Here, c denotes the speed of light and is used to translate clock offset differences from the time domain to the range domain for ease of interpretation.

At any epoch, the difference Δp of the observed-minus-computed pseudorange residuals using broadcast and precise ephemerides can then be expressed as

$$\Delta p = -\boldsymbol{e}^{\top}(\boldsymbol{r}^s_{\mathrm{bce,com}} - \boldsymbol{r}^s_{\mathrm{ref,com}}) + (\Delta\tau - \overline{\Delta\tau}) \tag{1}$$

where

$$\Delta\boldsymbol{r}^s = \boldsymbol{r}^s_{\mathrm{bce,com}} - \boldsymbol{r}^s_{\mathrm{ref,com}} \tag{2}$$

represents the orbit error of the broadcast ephemerides and $\boldsymbol{e}$ denotes the line-of-sight unit vector from the user to the satellite. For a given single-frequency user signal or a dual-frequency signal combination, both the broadcast and precise clock offset values need to be corrected for the respective group delay contribution as described by the pseudorange bias B. Accordingly,

✉ O. Montenbruck
oliver.montenbruck@dlr.de

[1] Deutsches Zentrum für Luft- und Raumfahrt, German Space Operations Center, 82234 Weßling, Germany

Published online: 05 December 2024

$$\Delta\tau = \left(cdt^s_{\mathrm{bce,com}} - B^s_{\mathrm{bce}}\right) - \left(cdt^s_{\mathrm{ref,com}} - B^s_{\mathrm{ref}}\right) \quad (3)$$

represents the error of the CoM-referenced and group-delay-corrected satellite clock offsets of the broadcast ephemeris. Here, systematic differences between the system time realization and the group delay reference are considered by removing the epoch-wise average $\overline{\Delta\tau}$ over all satellites in the constellation.

For a SISRE measure that is independent of the user location, it is common to consider the global average

$$s^2 \approx w_1^2\left(\Delta r_{\mathrm{R}} - \Delta\tau + \overline{\Delta\tau}\right)^2 + w_2^2\left(\Delta r_{\mathrm{A}}^2 + \Delta r_{\mathrm{C}}^2\right) \quad (4)$$

of the squared pseudorange error, which can be obtained by integration of Eq. (1) over the part of the Earth's surface in view of the satellite. Here, Δr_{R}, Δr_{A}, and Δr_{C} denote the components of the orbit error $\Delta\boldsymbol{r}^s$ in radial, along-track, and cross-track direction. The weight factors w_1 and w_2 depend on the orbit height of the GNSS satellite and the assumed elevation mask angle and can be computed using numerical or analytical relations as described in Dieter et al. (2004) and Renfro et al. (2024a). For GPS, a 2° elevation mask is adopted in DOD (2020), which results in values of $w_1 = 0.980$ and $w_2 = 0.141$. Weight factors for other representative elevation masks and orbit heights of other GNSS constellations are provided in Montenbruck et al. (2018) and Renfro et al. (2024a). RMS and 95th-percentile SISRE values can be obtained from Eq. (4) by forming the respective statistics of the epoch-wise global-average error s over a given period of interest. To separate the contribution of orbit errors from that of clock offset and bias errors, it is common to also consider the "orbit-only SISRE", which is obtained by neglecting $\Delta\tau$ and $\overline{\Delta\tau}$ in the above relation.

The latest version of the GPS Standard Positioning Service (SPS) performance standard released in 2020 (DOD 2020) specifies a 95th-percentile value of less than 7.0 m for the global-average SISRE during normal operations over all ages-of-data. This limit applies both for single-frequency L1 C/A-code and the legacy navigation message (LNAV) as well as dual-frequency L1 C/A plus L2C or L5 and the civil navigation message (CNAV). Assuming zero mean errors with a normal distribution, this is equivalent to a 3.6 m RMS SISRE value and presents a fairly conservative upper bound for the actual performance. In fact, SISRE values of less than 1 m were obtained as early as 2005 following completion of the legacy accuracy improvement initiative (L-AII; Creel et al. 2007), which introduced an improved orbit model and increased the number of monitoring stations available for orbit determination and time synchronization in the GPS control segment.

Over the following years, old Block IIA satellites were gradually replaced by modernized satellites with Rubidium atomic frequency standards (RAFSs). These offered enhanced stability over the clock prediction period required to cover the time between consecutive navigation message uploads, and resulted in a gradual SISRE improvement. For the 2013 to 2015 timeframe, RMS values of about 0.7 to 0.9m were achieved for single-frequency L1 users (Montenbruck et al. 2015b; Renfro et al. 2015; Perea et al. 2017), which further decreased over the following years and stabilized at roughly 0.6 m from 2019 onwards (Montenbruck et al. 2020; Renfro et al. 2024b). Even smaller values of about 0.4 to 0.5m apply for the Precise Positioning Service (DOD 2007) for dual-frequency P(Y) and LNAV users, which is not affected by group delay uncertainties (Fig. 1).

First announcements of a renewed performance enhancement initiative by the GPS providers were made in Hobbs (2024), who reported a decrease of the user range error for dual-frequency P(Y)-code users from an average of 45 cm in early 2024 to only 30 cm from March 2024 onwards. While no specific details were given, the enhancements were attributed to "clock swaps, additional uploads, troubleshooting noisy components, specialized commands".

For an independent characterization of these accuracy improvements, we first investigate relevant changes in the GPS space and control segment operations. As part of this, we discuss recent updates to the convention and numerical values of GPS transmit antenna phase center offsets for the orbit and clock offset determination and analyze the Allan deviation of the GPS satellite clocks to identify clock switches in the active constellation. Furthermore, we determine the epochs of navigation message uploads from broadcast ephemeris data of a global monitoring station network to characterize the upload pattern and to identify related changes. In a second step, we evaluate the GPS SISRE over a 20-months period (January 2023 to August 2024) considering different signal types and navigation message to quantify the recent performance improvements and to relate them to the previously discussed changes in the GPS operations.

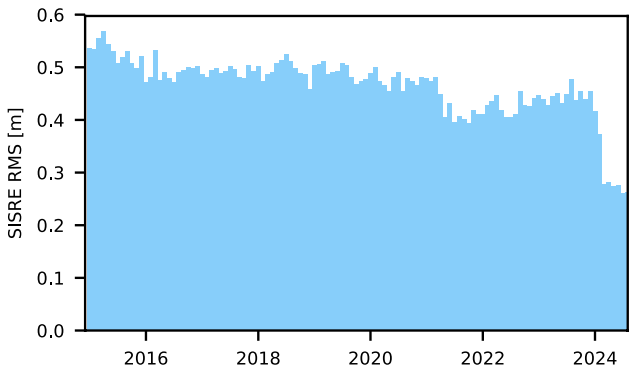

Fig. 1 Evolution of the monthly RMS SISRE between 2015 and 2024. All values refer to the Precise Positioning Service using dual-frequency P(Y) and LNAV navigation messages

Furthermore, the recent GPS SISRE performance is compared to Galileo and the global BeiDou-3 constellation. Finally, we provide a summary and conclusions addressing practical implications of the performance improvement and the relevance for GPS and multi-GNSS users.

GPS operational changes

Between fall 2023 and spring 2024 various changes in the operations of the GPS satellites have taken place which impact the overall system performance and its assessment. These comprise the active clocks, the upload intervals, and the phase center offsets.

Atomic frequency standards

Within the 2023/2024 time frame, the GPS constellation comprised four Blocks of GPS satellites (IIR, IIR-M, IIF, and III) equipped with different generations of RAFSs (Wu 1996; Dupuis et al. 2008) and, in case of Block IIF, a complementary Cesium (Cs) clock (Vannicola et al. 2010). The latter was in use on space vehicle number (SVN) G072 and G073, transmitting pseudorandom noise (PRN) codes G08 and G10, respectively, until early 2024. On February 9 of that year G073 transitioned to use of a Rb clock as the primary atomic frequency standard, followed by G072 near midnight of February 21/22 (Fig. 2). The clock swaps were not officially declared, but accompanied by generic Notices Advisories to NAVSTAR Users (NANUs; NAVCEN 2024a, b) marking the respective satellite as "unusable" for a period of about ten days after activation of the Rb clock. Furthermore, the Cs to Rb transitions are evident from a factor of ten reduction of the clock's Allan deviation over a wide range of time scales.

For the analysis of clock stability in the period of interest we made use of precise clock offset solution with 30 s sampling obtained by the Center for Orbit Determination in Europe (CODE) as part of their COD0OPSFIN product (Dach et al. 2023). Based on the respective data, overlapping Allan deviations (Riley 2008) were computed over consecutive seven-day intervals after correcting for day-boundary discontinuities and compensating possible secular trends by adjustment and subtraction of a second-order polynomial.

Results of the clock stability analysis are summarized in Fig. 3. It illustrates the statistical distribution of weekly Allan deviations (ADEVs) for correlation times of 4 h and 24 h, which correspond to the typical fit and upload intervals of GPS navigation data, respectively. In total, 34 different space vehicles were active in the 20-months period, which included handovers from SVN G041 to G044 and G063 to G049 for PRNs G22 and G01, respectively. Clear performance differences can be recognized between the different generations of RAFSs. Except for the IIF satellites, which suffer from thermally induced variations of the apparent clock phase (Montenbruck et al. 2012), the ADEV(4 h) results of each individual satellite show only a moderate scatter throughout the analysis period and range from 10^{-14} to 10^{-13} for the various RAFS types. On the other hand, peak values of 2×10^{-13} are reached for the IIF Cesium clocks. At the daily time scale, ADEVs of the Rubidum clocks are mostly at the 10^{-14} level, but a slightly larger scatter can be observed compared to the stability over 4-h intervals. Aside from the Cesium clock, below-average clock stabilities at 24 h may be noted for the RAFS of satellites G043, G048, G053, G057 and, most notably, G069.

As a rough approximation, stochastic clock variations over a period τ can be described by the expression $cdt(\tau) \approx c \cdot \mathrm{ADEV}(\tau) \cdot \tau$. For the 4-h fit interval, this yields representative errors ranging from a few centimeters to a few decimeters for the differences between the actual clock offsets and the adjusted clock polynomial. At the daily interval, which reflects the typical upload period for new sets of navigation messages, a 10^{-14} ADEV likewise implies a clock prediction error at the 0.25 m level, but notably larger errors may arise for the aforementioned satellites with unstable Rb or Cs clocks. Here, the limited clock stability implies a major constraint for the achievable SISRE and reduced upload intervals may be required for these satellites to maintain a uniform navigation data performance across the active constellation.

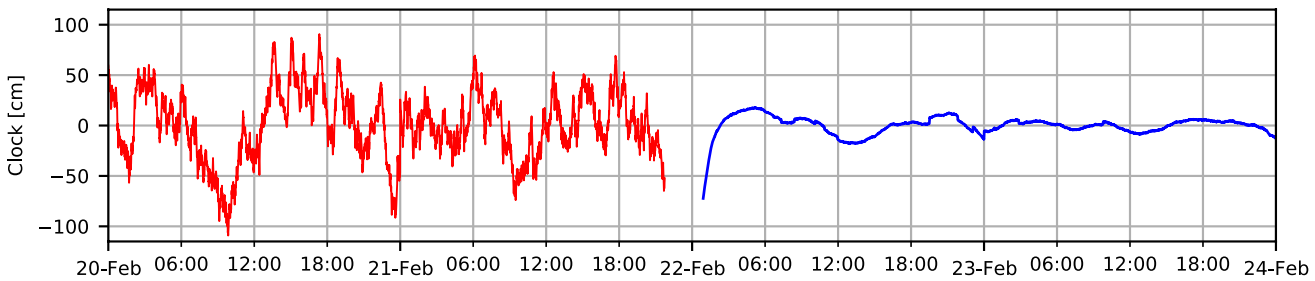

Fig. 2 Detrended clock offsets of satellite G072 across the Cesium (red) to Rubidium (blue) clock swap on February 21/22, 2024

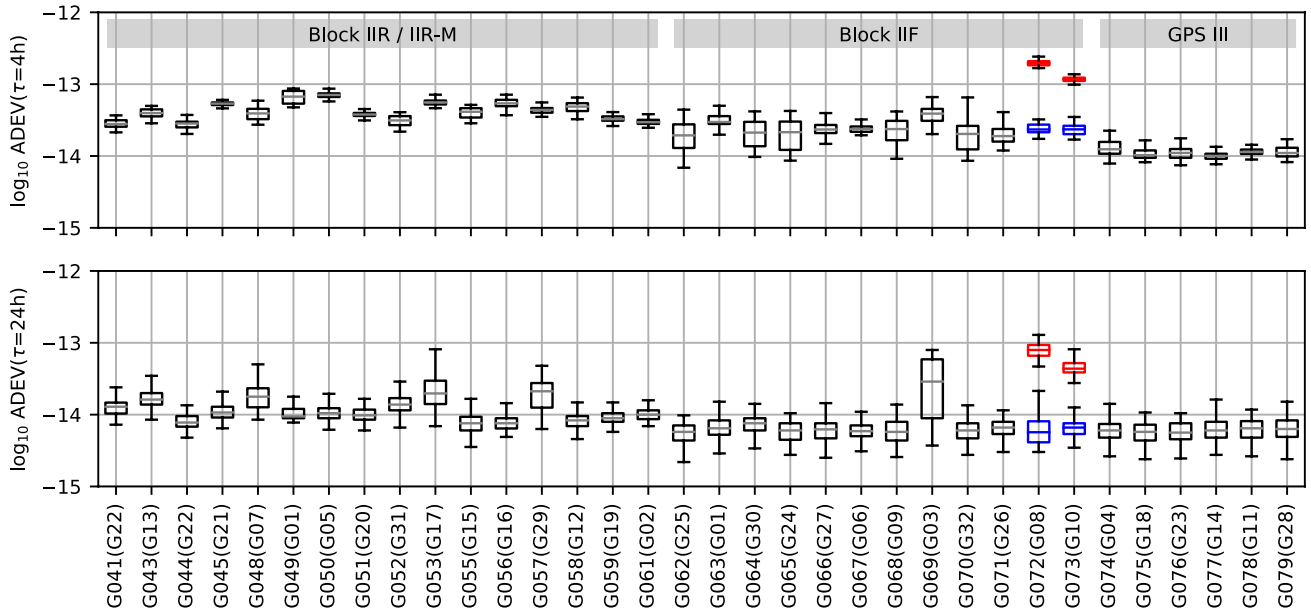

Fig. 3 Box-whisker plots illustrating the distribution of Allan deviations at $\tau = 14400$ s (top) and $\tau = 86400$ s (bottom) over consecutive 7-day intervals from January 2023 to August 2024. For SVN G072 and G073, distinct results are provided for dates before the Cs to Rb clock swaps in February 2024 (indicated by a red median value and inter-quartile range) and after the swap (in blue)

Upload interval

Following the ground-based orbit and clock determination in the GPS Master Control Station (MCS), the propagated orbit and clock data are approximated by the broadcast ephemeris model over consecutive time intervals with a two-hour shift in their reference epoch (Dorsey et al. 2017). These data are subsequently uploaded to the respective GPS satellite, which then transmits updated, but gradually aging, ephemeris data to the user. New uploads of refreshed orbit and clock data are traditionally performed once every day for each spacecraft in the constellation, even though more frequent uploads may be adopted for individual satellites with a degraded clock stability (Hegarty 2017).

The GPS Interface Control Document IS-GPS-200N for civil L1 and L2 signals (SSC 2022) specifies use of epoch values deviating from the nominal 2-hour grid (i.e., 0:00, 2:00, ..., 22:00 for LNAV and 01:30, 03:30, ..., 23:30 for CNAV) for the first (and occasionally second) element of each clock-ephemeris-integrity (CEI) data sequence. New batches of navigation messages from the same orbit and clock propagation can thus be identified from the condition that the ephemeris reference epoch t_{oe} differs from the immediately preceding navigation message and meets the condition

$$t_{oe} \bmod 7200\,\text{s} \neq \left\{ \begin{array}{c} 0\,\text{s} \\ 5400\,\text{s} \end{array} \right\} \text{for} \left\{ \begin{array}{c} \text{LNAV} \\ \text{CNAV} \end{array} \right\} \text{messages} .$$

The earliest transmit time t_{tm} of the respective ephemeris will then provide an approximation of the associated upload time.

Based on this methodology, LNAV and CNAV upload times between 1 January 2023 and 31 August 2024 were determined from the "BRD4" merged multi-GNSS broadcast ephemeris product (Montenbruck and Steigenberger 2022). Uploads of the CNAV messages on Block IIR-M and IIF satellites were found to follow those of LNAV messages with representative delays of 10 to 15 min, while matching upload times for both types of navigation messages were found on GPS III satellites. Over the examined time frame, uploads of new navigation data were performed within less than 25 hours after the preceding upload in 95% of all cases. The cumulative distribution function of the time between uploads is illustrated in Fig. 4 for epochs before and after 1 March 2024.

Prior to that date, the mean time between consecutive uploads ranged from 21.7 h to 23.3 h for most satellites of the GPS constellation. As an exception, almost two uploads were performed each day for the two Block IIF satellites SVN(PRN) G069(G03) and G072(G08). For these satellites, the mean times between consecutive uploads amounted to 14 h and 13 h, respectively.

Starting in March 2024, additional upload capacity from other missions was made available for GPS to reduce the mean upload interval on a notably larger number of GPS satellites. Overall, a total of ten IIR, IIR-M and IIF satellites (SVN G043, G045, G048, G052, G053, G057, G061, G069,

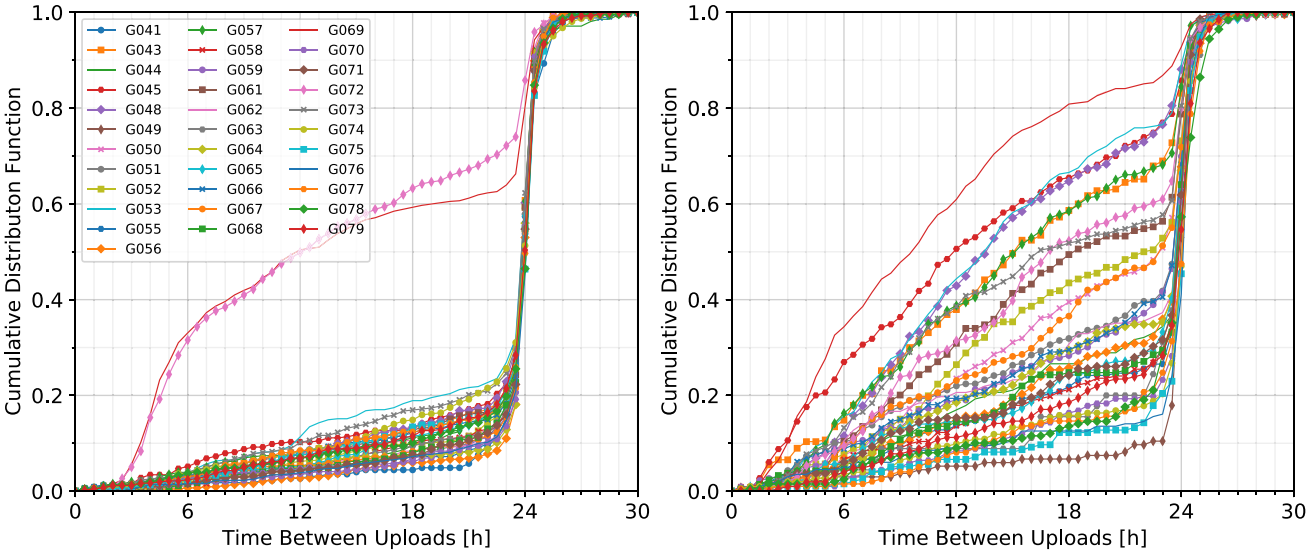

Fig. 4 Cumulative distribution of the time between consecutive GPS navigation message uploads from January 2023 to Feb 2024 (left) and from March to August 2024 (right)

G072, G073) now benefit from a reduced mean upload time of about 11 h to 18 h. This group corresponds closely to the set of satellites with a median ADEV(24 h) of more than 1×10^{-14} (Fig. 3), which may cause differences of true and predicted clock offsets at the 1-m level after a 1-day forecast interval. Interestingly, satellites G072 and G073 are both still considered for the increased update rate, even though their clock stability at daily intervals is well below that threshold after the switch from Cesium to Rubidium clocks and fully comparable to the nominal performance of other Block IIF and GPS III satellites operating on RAFS.

Phase center offsets

Satellite positions and clock offsets transmitted in the GPS navigation message are jointly referred to a common reference point representing the antenna phase center. Within the GPS MCS, satellite-specific, conventional values for the offset between this phase center and the satellite's CoM are applied as part of the orbit determination and ephemeris generation. Knowledge of these phase center offsets (PCOs) is not required for pseudorange modeling from broadcast ephemerides in the user receiver, but affects the comparison with precise ephemerides providing CoM-based orbits and clock offsets relative to different models of the antenna phase center and phase variations.

As first disclosed in Malys et al. (2021), the PCOs used in the MCS were consistent since 1989 with values adopted by the National Geospatial Agency (NGA) and documented in, e.g., NGA (2014) and NGA (2020). While the exact nature and origin of the legacy NGA/MCS PCOs is no longer traceable, the values are likely to represent manufacturer calibrations of the L1 phase centers (Montenbruck et al. 2024). As of January 3, 2021 a new realization WGS84(G2139) of the World Geodetic System 84 was released and implemented (NGA 2021) to improve the overall alignment with the International Terrestrial Reference Frame (ITRF). With a three-months delay, NGA and the GPS MCS furthermore decided to adopt PCOs for the ionosphere-free L1/L2 combination based on the antenna model of the International GNSS Service (IGS; Johnston et al. 2017) for best compatibility with the ITRF GNSS contribution. The new PCO values were introduced on 28 March 2021 (GPS week 2151) and taken from the latest version igs14_2134.atx of the IGS antenna model available at that time. As an exception, L1 manufacturer calibrations were adopted for the GPS III satellites. Along with the release of the most recent WGS realization, WGS84(G2296), NGA and the MCS once again updated the PCOs for GPS orbit determination and ephemeris generation in January 2024 (NGA 2024). This time, L1/L2 PCOs from the igs20_2290.atx antenna model were adopted for all operational GNSS satellites to ensure best compatibility of the WGS84(G2296) reference frame with the ITRF2020 (Altamimi et al. 2023) realization of the International Terrestrial Reference System. For further reference, a summary of PCO values as used by the MCS is given in Table 1.

Performance analysis

For our analysis, we consider the SISRE evolution for four different combinations of user signals and navigation messages, that are summarized in Table 2. Case A

Table 1 Antenna phase center offsets for GPS navigation message generation (NGA 2020, 2021, 2024). All values refer to IGS conventions for the spacecraft body coordinate system (Montenbruck et al. 2015a)

SVN	Block	Until 2021/03/28			2021/03/28 – 2024/01/07			From 2024/01/07		
		x [m]	y [m]	z [m]	x [m]	y [m]	z[m]	x [m]	y [m]	z [m]
G041	IIR-A	−0.002	0.000	+1.614	−0.003	−0.002	+1.305	−0.003	−0.002	+1.237
G043	IIR-A	−0.002	−0.003	+1.614	−0.002	−0.002	+1.348	−0.002	−0.002	+1.287
G044	IIR-A	−0.002	−0.001	+1.513	+0.001	+0.005	+1.000	+0.001	+0.005	+0.936
G045	IIR-A	−0.002	+0.001	+1.584	−0.003	+0.003	+1.359	−0.003	+0.003	+1.290
G046	IIR-A	−0.002	−0.001	+1.514	−0.001	−0.001	+1.118	−0.001	−0.001	+1.054
G047	IIR-B	−0.002	+0.001	+0.060	−0.002	+0.002	+0.851	−0.002	+0.002	+0.771
G048	IIR-M	−0.001	0.000	+0.001	0.000	+0.005	+0.822	0.000	+0.005	+0.757
G049	IIR-M	−0.012	0.000	−0.023	0.000	0.000	+0.963	0.000	0.000	+0.865
G050	IIR-M	−0.003	0.000	−0.017	−0.003	0.000	+0.778	−0.003	0.000	+0.743
G051	IIR-A	−0.002	−0.001	+1.614	+0.001	−0.003	+1.314	+0.001	−0.003	+1.262
G052	IIR-M	−0.002	0.000	−0.058	−0.001	+0.006	+0.913	−0.001	+0.006	+0.837
G053	IIR-M	+0.010	−0.006	−0.101	+0.003	+0.001	+0.771	+0.003	+0.001	+0.712
G054	IIR-A	+0.010	−0.006	+1.592	+0.014	0.000	+1.249	+0.014	0.000	+1.182
G055	IIR-M	+0.010	−0.006	−0.012	+0.005	+0.002	+0.623	+0.005	+0.002	+0.576
G056	IIR-A	+0.010	−0.006	+1.663	+0.013	−0.007	+1.469	+0.013	−0.007	+1.389
G057	IIR-M	+0.010	−0.006	−0.015	+0.011	−0.005	+0.792	+0.011	−0.005	+0.723
G058	IIR-M	+0.010	−0.006	−0.094	+0.010	−0.006	+0.768	+0.010	−0.006	+0.711
G059	IIR-B	+0.008	−0.005	−0.018	+0.009	−0.001	+0.808	+0.009	−0.001	+0.719
G060	IIR-B	+0.009	−0.004	0.000	+0.015	+0.007	+0.766	+0.015	+0.007	+0.702
G061	IIR-B	+0.010	−0.006	−0.082	+0.001	−0.001	+0.729	+0.001	−0.001	+0.682
G062	IIF	+0.392	+0.002	+1.093	+0.394	0.000	+1.517	+0.394	0.000	+1.454
G063	IIF	+0.391	0.000	+1.091	+0.394	0.000	+1.502	+0.394	0.000	+1.421
G064	IIF	+0.395	−0.001	+1.090	+0.394	0.000	+1.522	+0.394	0.000	+1.462
G065	IIF	+0.392	+0.002	+1.093	+0.394	0.000	+1.407	+0.394	0.000	+1.352
G066	IIF	+0.391	0.000	+1.090	+0.394	0.000	+1.522	+0.394	0.000	+1.436
G067	IIF	+0.395	−0.001	+1.092	+0.394	0.000	+1.467	+0.394	0.000	+1.411
G068	IIF	+0.396	−0.002	+1.092	+0.394	0.000	+1.523	+0.394	0.000	+1.460
G069	IIF	+0.395	0.000	+1.091	+0.394	0.000	+1.551	+0.394	0.000	+1.482
G070	IIF	+0.397	0.000	+1.084	+0.394	0.000	+1.535	+0.394	0.000	+1.472
G071	IIF	+0.393	−0.001	+1.093	+0.394	+0.000	+1.504	+0.394	+0.000	+1.434
G072	IIF	+0.396	+0.000	+1.086	+0.394	+0.000	+1.501	+0.394	+0.000	+1.428
G073	IIF	+0.396	−0.001	+1.083	+0.394	+0.000	+1.515	+0.394	+0.000	+1.429
G074	III	−0.059	+0.018	+1.090	−0.059	+0.018	+1.090	−0.061	+0.020	+1.940
G075	III	−0.073	+0.021	+1.074	−0.073	+0.021	+1.074	−0.064	+0.015	+1.940
G076	III	−0.065	+0.020	+1.062	−0.065	+0.020	+1.062	−0.069	+0.022	+1.920
G077	III	−0.064	+0.023	+1.099	−0.064	+0.023	+1.099	−0.066	+0.019	+1.939
G078	III				−0.066	+0.023	+1.102	−0.068	+0.021	+1.965
G079	III				−0.066	+0.023	+1.113	−0.068	+0.021	+1.965

Table 2 Navigation message types and user signals considered for the GPS SISRE analysis

Case	Navigation Msg	Signals
A	LNAV	L1 C/A
B		L1 P(Y), L2 P(Y)
C	CNAV	L1 C/A
D		L1 C/A, L2C

represents the legacy definition of the Standard Positioning Service using L1 C/A code observations along with the LNAV message. As of 2024, these are still the only civil signals and data transmitted by the entire GPS constellation, even though more than three quarters of all satellites already offer the new civil L2C signal and CNAV message for dual-frequency positioning. Use of that processing mode has officially been introduced into the 2020 edition of the SPS performance standard (DOD 2020) and is considered as Case D in this work. We contrast this

mode with dual-frequency positioning using L1 and L2 P(Y)-code signals in Case B. While formally assigned to the regulated Precise Positioning Service (PPS; (DOD 2007), P(Y) signals are available on all satellites of the GPS constellation and semi-codeless tracking enables access to P(Y)-code tracking also for civil receivers without decryption devices. Case C, finally, considers single frequency L1 navigation but using CNAV navigation messages. While this reflects a largely hypothetical scenario, in which users would have access to the L2 (or L5) CNAV message but still perform L1-only positioning, it appears instructive to demonstrate the vital role of the L1 C/A-to-P(Y) group delay differences on the C/A pseudorange modeling performance.

In view of a larger number of parameters and higher resolution, the CNAV orbit model offers a better goodness-of-fit and lower discontinuities at ephemeris handovers than LNAV (Steigenberger et al. 2015). Nevertheless, both navigation messages offer a largely compatible overall orbit and clock performance, which is driven by the forecast accuracy in the MCS. As such, differences in the SISRE performance between the various services are mainly related to the availability and quality of group delay parameters for individual user signals.

Single- and dual-frequency SISRE

Monthly SISRE values covering January 2023 to August 2024 are shown in Fig. 5 for the various combinations of signals and navigation messages. All results are based on the BRD4 merged multi-GNSS broadcast ephemerides (Montenbruck and Steigenberger 2022) and the COD0MGXFIN precise orbit and clock products of the Center for Orbit Determination in Europe (Dach et al. 2024), as well as the CAS0OPSRAP bias products of the Chinese Academy of Sciences (Wang et al. 2016).

Prior to February 2024, the SPS (Case A) and PPS (Case B) SISREs amount to roughly 55 cm and 45 cm RMS, respectively. Both positioning services assume use of the LNAV navigation message and are supported by the entire GPS constellation, but differ in the choice of user signals (L1 C/A-code vs. L1/L2 P(Y) code). Other than might be expected at first sight, the choice of single- vs. dual-frequency signals has no direct impact on the degraded SPS results, since SISRE values consider only the space and control segment contributions to the user range model, but no ionospheric errors. Instead, the PPS SISRE benefits from the fact that no group delay uncertainties need to be considered, since the user signals match the signals used in the determination of the broadcast clock offsets. C/A-code users, in contrast, require knowledge of the L1 C/A vs. L1/L2 P(Y)

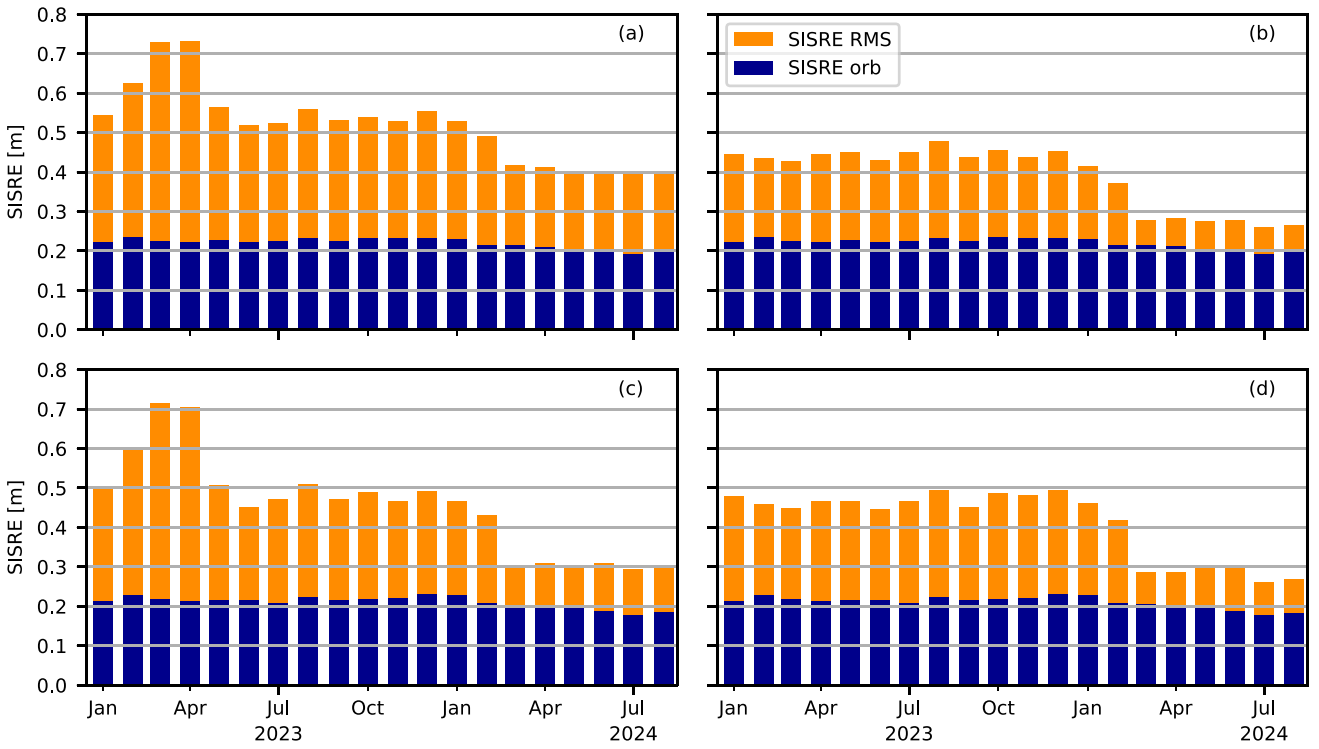

Fig. 5 RMS SISRE and SISRE(orb) for four different combinations of user signals and navigation messages. (a) L1 C/A, LNAV; (b) L1 P(Y), L2 P(Y), LNAV; (c) L1 C/A, CNAV; (d) L1 C/A, L2C, CNAV

group delays. However, only the L1 P(Y) vs. L1/L2 P(Y) group delay is provided in the LNAV message as part of the Timing Group Delay (TGD) parameter. The residual L1 C/A vs. L1 P(Y) group delays (known as L1 C/A inter-signal corrections, ISCs) are unavailable to LNAV users, exhibit representative magnitudes of up to ±2 ns or ±0.6 m (Wang et al. 2016), causing a notable SISRE increase compared to the PPS.

With roughly 50 cm, the SISREs for use of civil signals and the CNAV navigation message (Cases C and D) are slightly larger than the PPS SISRE, but clearly superior to the legacy SPS (Case A). Even though these cases do not include use of old IIR satellites with potentially inferior clock stability, they mainly benefit from availability of all relevant ISCs in the CNAV message. This can readily be seen from the nearly identical results of the dual-frequency CNAV SISRE (Case C) and the (hypothetical) SISRE for single-frequency L1 C/A + CNAV users.

Overall, the SISRE prior to the performance improvement is dominated by the contributions of clock instabilities and, in the case of the L1 C/A LNAV users, by unknown group delays. As indicated by the orbit-only SISRE of about 20 cm, uncertainties in the predicted orbits contribute only a minor part to the root-sum-square (RSS) of all error sources, leaving roughly 40 to 55cm to the clock and bias errors in the navigation messages.

For completeness, we also note that the larger-than-average L1-only SISRE values of 0.7 to 0.8m in early 2023 are related to the latest GPS III satellite SVN G079. This satellite was set healthy in mid February 2023, but transmitted an improper TGD causing a range error of about 3 m until May 4, 2023, when the correct TGD was made available. While users might have eliminated the affected satellite as part of the receiver autonomous integrity monitoring (RAIM), it was part of the active GPS constellation at that time and has therefore been included into the SISRE analysis.

Following the operational changes described in the previous section, a pronounced SISRE decrease can be recognized from March 2024 onward. It is most evident for PPS and CNAV users while the benefits are still largely masked by the lacking group delays information for civil L1 users. Even though the increased upload rate results also in a small ($\approx 10\,\%$) reduction of the orbit-only SISRE, the dominating benefit is clearly related to the reduction of clock prediction errors. In fact, the total PPS SISRE reaches a level of roughly $\sqrt{2}$ times the orbit-only SISRE after implementation of the accuracy improvement initiative, thus indicating an almost equal RSS contribution of orbit and clock prediction errors to the overall SISRE across the entire constellation.

For further reference, SISRE values for single- and dual-frequency Galileo and BeiDou-3 are provided in Table 3 for a one-month period in mid 2024. They are based on comparison of the respective broadcast orbit, clock, and group delay parameters with the COD0MGXFIN multi-GNSS orbit and clock products (Dach et al. 2024) and the CAS0OPSRAP code biases (Wang et al. 2016). While Galileo clearly outperforms the other GNSSs in terms of SISRE, the results show that GPS has caught up, and is again second place before BeiDou-3. In particular, the GPS SISRE for dual-frequency users is clearly lower than that of the Chinese navigation system, even though BeiDou-3 benefits from very stable clocks as well as inter-satellite links enabling hourly navigation message uploads. On the other hand, these benefits are counteracted by intrinsic incompatibilities of the BeiDou-3 time synchronization and group delay parameters with actual user receivers (Montenbruck et al. 2022).

Table 3 Comparison of SISRE values for single- and dual-frequency navigation of GPS, Galileo, and BeiDou-3 in August 2024

GNSS	Signals	Nav. Msg	SISRE (RMS) [m]
GPS	L1 C/A	LNAV	0.40
	L1 C/A, L2C	CNAV	0.27
	L1/L2 P(Y)	LNAV	0.26
Galileo	E1	INAV	0.23
	E1, E5a	FNAV	0.11
BeiDou-3	B1C	CNAV-1	0.44
	B1C, B2a	CNAV-1	0.47

Cui Bono – who benefits?

Evidently, the SISRE reduction achieved by selecting more stable onboard clocks and by increasing the navigation message upload frequency marks a major improvement and increases the competitiveness of GPS in comparison with other GNSSs. Nevertheless, it appears worthwhile to ask, which applications specifically would benefit from this enhancement and how the SISRE reduction would materialize in the resulting positioning accuracy.

In this context, it is recalled that the concepts of SISRE, UEE, and dilution of precision (DOP) have been developed as a framework for assessing the performance pseudorange-based single-point positioning and for characterizing individual contributions to the overall error budget. Leaving aside the number and geometric distribution of satellites, the SPP accuracy is driven by errors in the observed and modelled measurements, which are described as the RSS of signal-in-space range errors and user equipment errors. While continued improvements in the space and ground segment have contributed to a SISRE reduction down to the few-decimeter level, the UEEs have not improved in a similar manner. Even though the pseudorange noise of survey- and geodetic-grade receivers with wide-band frontends may reach a level of one or a few decimeters for uncombined

observations, the uncertainties of ionospheric models contribute notably larger errors in single-frequency positioning. Vice versa, dual-frequency navigation is essentially free of ionospheric errors but suffers from the unfavorable amplification of noise and multipath errors (by roughly a factor of three; Hauschild 2017) when forming the ionosphere-free linear combination. As a result, SPP errors are typically dominated by the UEE contribution, and even a notable SISRE reduction as achieved in the latest GPS accuracy improvement initiative does not show up in a corresponding improvement of the positioning error budget.

By way of example, this is illustrated in Fig. 6, which shows the distribution of single-point positioning errors for a representative geodetic reference station. All results are based on dual-frequency P(Y)-code observations considering a 10° elevation mask and a maximum position dilution of precision (PDOP) of 10. Individual positioning solutions for the Brussels station of the IGS were computed at 30 s steps for five-day intervals centered around day of year (DoY) 30/2024 and 60/2024, respectively, and are based on LNAV messages and dual-frequency P(Y) observations. The two dates roughly mark the begin and end of the operational changes implemented in early 2024 to reduce the SISRE of the GPS constellation. Within this period, the horizontal position errors of the BRUX station decreased by roughly 8%, out of which 3% can be attributed to a slightly more

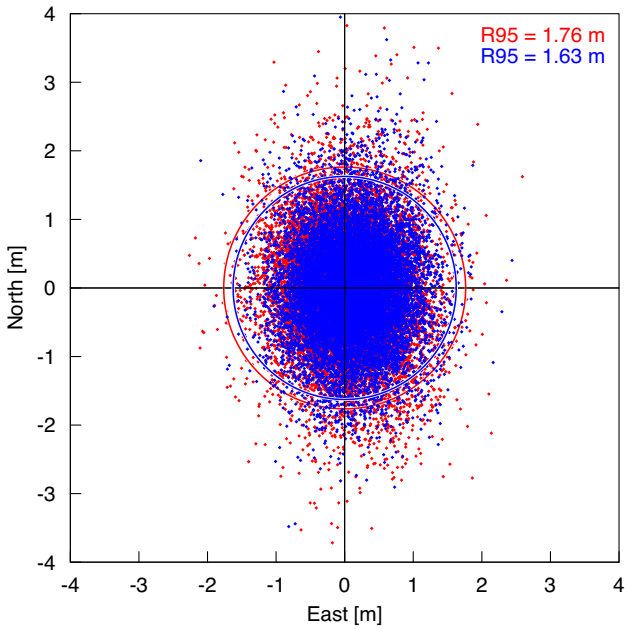

Fig. 6 Scatter of horizontal SPP errors for the IGS BRUX station before (blue) and after (red) implementation of the 2024 accuracy improvement initiative. The 95th percentile radii (R95) are indicated by solid circles in the corresponding colors and amount to roughly 1.7 times the distance root mean square (DRMS) horizontal position error

favorable dilution of precision at the end of February. The user equivalent range errors (UEREs), i.e., the RSSs of SISRE and UEE, in the two periods amount to roughly 0.90 m and 0.86 m, respectively. They are dominated by a UEE of roughly 0.80 m, which exceeds the SISRE values by a factor of two to three and largely masks the SISRE improvement.

Given the magnitude of representative pseudorange measurement errors, the SISRE performance of GPS, Galileo, and BeiDou-3 has only limited impact on the achievable SPP accuracy and is thus barely distinguishable in practice. As such, precise point positioning (PPP; Zumberge et al. 1997) techniques based on dual-frequency carrier phase observations are required to fully materialize the benefits of today's low SISRE values. Other than single point positioning, PPP requires the adjustment of carrier phase ambiguities collecting information from multiple epochs. On the other hand, carrier-phase-related UEEs are essentially negligible, when using PPP techniques with broadcast ephemerides. Furthermore, ephemeris errors can in part by compensated through dedicated error states or process noise in a sequential filter (Gunning et al. 2019; Carlin et al. 2021). While PPP with broadcast ephemerides has received only limited attention so far, selected studies (Hadas et al. 2019; Carlin et al. 2021; Cheng et al. 2024) have demonstrated the feasibility of decimeter-level positioning with overall errors proportional to the constellation-specific SISRE values.

Sample PPP results using LNAV navigation messages and dual-frequency P(Y) carrier phase observations in a kinematic positioning mode are collated in Table 4 and compared with SPP solutions for the previously considered test periods. At a horizontal dilution of precision (HDOP) close to one, the resulting DRMS position errors essentially match the UERE in all four cases. Other than the SPP solutions, which are dominated by UEE contributions, the PPP solutions are essentially free of receiver-related measurement errors and directly reflect the SISRE improvement achieved in early 2024.

While the GPS SISRE enhancement offered by the recent GPS accuracy improvement initiative obviously contributes to a reduced positioning error budget, it appears unlikely to affect the relevance of satellite-based correction services such provides by Satellite Based

Table 4 Horizontal positioning errors (DRMS) of the BRUX station using code- and carrier-phase-based positioning techniques for five-day periods before and after implementation of the GPS accuracy improvements

Period (DoY)	DRMS(SPP) [m]	DRMS(PPP) [m]
28 – 32/2024	0.96	0.43
58 – 62/2024	0.89	0.30

Augmentation Systems (SBAS; Walter 2017) or the Galileo High Accuracy Service (HAS; Fernandez-Hernandez et al. 2022). Aside from integrity information for aviation users, the main benefits of SBAS for positioning stem from the availability of ionospheric corrections for single-frequency processing, which typically exceed the orbit and clock errors by an order of magnitude. For PPP users, HAS still offers a somewhat lower GPS SISRE than the uncorrected navigation message even after the performance improvement, and, foremost, group delay corrections for the relevant user signals of all GPS satellites.

Summary and conclusions

Various operational changes have led to a notable performance improvement in the GPS Standard Positioning Service in early 2024. These are achieved by selecting the most stable onboard clocks on each spacecraft and by increasing the mean upload interval for satellites with less-than-average clock stability. Overall, the global-average signal-in-space range error could be decreased from roughly 45 cm to 30 cm for dual-frequency P(Y) and L1 C/A + L2C users along with the LNAV and CNAV navigation messages, respectively. Slightly larger values of about 40 cm after February 2024 apply for single-frequency L1 C/A-code users due the lack of relevant inter-signal group delay corrections in the LNAV message. Compared to other GNSSs, GPS again outperforms BeiDou-3 in terms of control and space segment contributions to the ranging error, but still falls behind Galileo by a factor of two to three. On the other hand, SISRE values for all three constellations are well below representative user equipment errors. As such, carrier-phase-based positioning techniques would be required to fully exploit the quality of the respective navigation messages in all cases.

Acknowledgements The International GNSS Service (IGS) is acknowledged for providing GNSS observation data and navigation messages. Precise orbit, clock and bias products were contributed by the Center for Orbit Determination in Europe (CODE) and the Chinese Academy of Sciences (CAS).

Author contributions OM developed the study concept and prepared the initial manuscript. PS and OM contributed to the data analysis as well as the graphical representation, discussion and interpretation of results. Both authors critically reviewed the final manuscript.

Funding Open Access funding enabled and organized by Projekt DEAL, an initiative of the Alliance of Science Organisations in Germany.

Data availibility GNSS observation data, navigation messages, and precise products used in this study are publicly available from the global IGS data centers, such as CDDIS (https://cddis.nasa.gov/archive/gnss/data/).

Declarations

Conflict of interest The authors have no Conflict of interest that are relevant to the content of this article.

References

Altamimi Z, Rebischung P, Collilieux X, Métivier L, Chanard K (2023) ITRF2020: an augmented reference frame refining the modeling of nonlinear station motions. J Geod 97(5):47. https://doi.org/10.1007/s00190-023-01738-w

Bernstein H (1983) Calculations of user range error (URE) variance from a Global Positioning (GPS) satellite, Aerospace Corporation, Rep. No. TOR-0083(3476-02)-1

Carlin L, Hauschild A, Montenbruck O (2021) Precise point positioning with GPS and Galileo broadcast ephemerides. GPS Solut 25(2):77. https://doi.org/10.1007/s10291-021-01111-4

Cheng Q, Chen J, Zhang Y, Yu C (2024) Real-time precise point positioning method considering broadcast ephemeris discontinuities. NAVIGATION: J Inst Nav, https://doi.org/10.33012/navi.643

Creel T, Dorsey AJ, Mendicki PJ, Little J, Mach RG, Renfro BA (2007) Summary of accuracy improvements from the GPS legacy accuracy improvement initiative (L-AII). In: Proc ION GNSS 2007:2481–2498

Dach R, Schaer S, Arnold D, Brockmann E, Kalarus M, Prange L, Stebler P, Jaeggi A (2023) CODE final product series for the IGS. https://doi.org/10.48350/185744

Dach R, Schaer S, Arnold D, Brockmann E, Kalarus MS, Lasser M, Stebler P, Jaeggi A (2024) CODE product series for the IGS-MGEX project. https://doi.org/10.48350/185744

Dieter GL, Hatten GE, Taylor J (2004) MCS zero age of data measurement techniques. In: 35th Annual Precise Time and Time Interval (PTTI) Meeting, PTTI, pp 103–116

DOD (2007) Global Positioning System Precise Positioning Service Performance Standard, 1st edn. Department of Defense, https://www.gps.gov/technical/ps/2020-SPS-performance-standard.pdf

DOD (2020) Global Positioning System Standard Positioning Service Performance Standard, 5th edn. Department of Defense, https://www.gps.gov/technical/ps/2020-SPS-performance-standard.pdf

Dorsey AJ, Marquis WA, Betz JW, Hegarty CJ, Kaplan ED, Ward PW, Pavloff MS, Fyfe PM, Milbert D, Wiederholt LF (2017) Global Positioning System. In: Kaplan ED, Hegarty C (eds) Understanding GPS/GNSS: principles and applications. Artech House

Dupuis RT, Lynch TJ, Vaccaro JR (2008) Rubidium frequency standard for the GPS IIF program and modifications for the RAFSMOD program. In: IEEE International Frequency Control Symposium, pp 655–660, https://doi.org/10.1109/FREQ.2008.4623081

Fernandez-Hernandez I, Chamorro-Moreno A, Cancela-Diaz S, Calle-Calle JD, Zoccarato P, Blonski D, Senni T, de Blas FJ, Hernández C, Simón J, Mozo A (2022) Galileo high accuracy service: initial

definition and performance. GPS Solut. https://doi.org/10.1007/s10291-022-01247-x
Gunning K, Blanch J, Walter T (2019) SBAS corrections for PPP integrity with solution separation. In: Proc. ION ITM 2019, p 707–719, https://doi.org/10.33012/2019.16739
Hadas T, Kazmierski K, Sośnica K (2019) Performance of Galileo-only dual-frequency absolute positioning using the fully serviceable Galileo constellation. GPS Solut 23(4):108. https://doi.org/10.1007/s10291-019-0900-9
Hauschild A (2017) Combinations of observations. In: Teunissen PJ, Montenbruck O (eds) Springer Handbook of Global Navigation Satellite Systems, Springer, chap 20, pp 583–604, https://doi.org/10.1007/978-3-319-42928-1_20
Hegarty CJ (2017) The Global Positioning system (GPS). In: Teunissen PG, Montenbruck O (eds) Springer Handbook of Global Navigation Satellite Systems, Springer, chap 7, pp 197–218,https://doi.org/10.1007/978-3-319-42928-1_7
Hobbs S (2024) Global Positioning System Update to the ENC. In: European Navigation Conference (ENC 2024)
Johnston G, Riddell A, Hausler G (2017) The International GNSS Service. In: Teunissen PG, Montenbruck O (eds) Springer Handbook of Global Navigation Satellite Systems, Springer, chap 33, pp 967–982, https://doi.org/10.1007/978-3-319-42928-1_33
Langley R, Teunissen P, Montenbruck O (2017) Introduction to GNSS. In: Teunissen P, Montenbruck O (eds) Springer Handbook of Global Navigation Satellite Systems, Springer, chap 1, pp 3–23, https://doi.org/10.1007/978-3-319-42928-1_1
Malys S, Solomon R, Drotar J, Kawakami T, Johnson T (2021) Compatibility of terrestrial reference frames used in GNSS broadcast messages during an 8-week period of 2019. Adv Space Res 67(2):834–844. https://doi.org/10.1016/j.asr.2020.11.029
Montenbruck O, Steigenberger P (2022) BRD400DLR: DLR's merged multi-GNSS broadcast ephemeris product in RINEX 4.00 format; DLR/GSOC. https://doi.org/10.57677/BRD400DLR
Montenbruck O, Hugentobler U, Dach R, Steigenberger P, Hauschild A (2012a) Apparent clock variations of the Block IIF-1 (SVN62) GPS satellite. GPS Solut 16:303–313. https://doi.org/10.1007/s10291-011-0232-x
Montenbruck O, Schmid R, Mercier F, Steigenberger P, Noll C, Fatkulin R, Kogure S, Ganeshan AS (2015) GNSS satellite geometry and attitude models. Adv Space Res 56(6):1015–1029. https://doi.org/10.1016/j.asr.2015.06.019
Montenbruck O, Steigenberger P, Hauschild A (2015b) Broadcast versus precise ephemerides: a multi-GNSS perspective. GPS Solut 19:321–333. https://doi.org/10.1007/s10291-014-0390-8
Montenbruck O, Steigenberger P, Hauschild A (2018) Multi-GNSS signal-in-space range error assessment - methodology and results. Adv Space Res 61(12):3020–3038. https://doi.org/10.1016/j.asr.2018.03.041
Montenbruck O, Steigenberger P, Hauschild A (2020) Comparing the 'Big 4-a user's view on GNSS performance. In: IEEE/ION Position, Location and Navigation Symposium (PLANS), pp 407–418, https://doi.org/10.1109/PLANS46316.2020.9110208
Montenbruck O, Steigenberger P, Wang N, Hauschild A (2022) Characterization and performance assessment of BeiDou-2 and BeiDou-3 satellite group delays. NAVIGATION: J Inst Nav 69(3), https://doi.org/10.33012/navi.526
Montenbruck O, Steigenberger P, Mayer-Gürr T (2024) Manufacturer calibrations of GPS transmit antenna phase patterns: a critical review. J Geod 98(1):2. https://doi.org/10.1007/s00190-023-01809-y
NAVCEN (2024a) Notices Advisory to NAVSTAR Users (NANU) 2024008. https://www.navcen.uscg.gov/sites/default/files/gps/nanu/2024/2024008.nnu
NAVCEN (2024b) Notices Advisory to NAVSTAR Users (NANU) 2024010. https://www.navcen.uscg.gov/sites/default/files/gps/nanu/2024/2024010.nnu
NGA (2014) NGA GPS ephemeris/station/antenna offset documentation; effective date November 1, 2014. https://web.archive.org/web/20141128063431/http://earth-info.nga.mil:80/GandG/satthtml/gpsdoc2014_11a.html
NGA (2020) NGA GNSS division precise ephemeris parameters; February 20, 2020. https://earth-info.nga.mil/php/download.php?file=gnss-precise
NGA (2021) (U) Recent update to WGS 84 reference frame and NGA transition to IGS ANTEX. https://earth-info.nga.mil/php/download.php?file=(U)WGS%2084(G2139).pdf
NGA (2024) WGS 84 (G2296) terrestrial reference frame realization. https://earth-info.nga.mil/php/download.php?file=WGS%2084(G2296).pdf
Perea S, Meurer M, Rippl M, Belabbas B, Joerger M (2017) URA/SISA analysis for GPS and Galileo to support ARAIM. Navigation J Inst Nav 64(2):237–254. https://doi.org/10.1002/navi.199
Renfro B, Drotar J, Finn A, Stein M, Reed E, Villalba E (2024a) An analytical derivation of the signal-in-space root-mean-square user range error. NAVIGATION: J Inst Nav 71(1), https://doi.org/10.33012/navi.630
Renfro BA, King J, Terry A, Kammerman J, Munton D, York J (2015) An analysis of Global Positioning System Standard Positioning System performance for 2013 (TR SGL-15-02). Applied Research Laboratories, University of Texas at Austin. https://www.gps.gov/systems/gps/performance/2013-GPS-SPS-performance-analysis.pdf
Renfro BA, Stein M, B RE, Austin F (2024b) An analysis of Global Positioning System Standard Positioning Service performance for 2020 (TR SGL-23-02). Applied Research Laboratories, University of Texas at Austin. https://www.gps.gov/systems/gps/performance/2022-GPS-SPS-performance-analysis.pdf
Riley WR (2008) Handbook of frequency stability analysis (SP 1065). National Institute of Standards and Technology, Boulder CO
SSC (2022) NAVSTAR GPS Space Segment/Navigation User Segment Interfaces, IS-GPS-200, rev. N, 22 Aug. 2022, Space Systems Command (SSC). https://www.gps.gov/technical/icwg/IS-GPS-200N.pdf
Steigenberger P, Montenbruck O, Hessels U (2015) Performance evaluation of the early CNAV navigation message. NAVIGATION: J Inst Nav 62(3):219–228. https://doi.org/10.1002/navi.111
Vannicola F, Beard R, White J, Senior K, Largay M, Buisson J (2010) GPS Block IIF atomic frequency standard analysis. In: Proc 42nd PTTI Meeting, pp 181–196
Walter T (2017) Satellite Based Augmentation Systems. In: Teunissen PG, Montenbruck O (eds) Springer Handbook of Global Navigation Satellite Systems, Springer, chap 12, pp 339–361, https://doi.org/10.1007/978-3-319-42928-1_12
Wang N, Yuan Y, Li Z et al (2016) Determination of differential code biases with multi-GNSS observations. J Geod 90(3):209–228. https://doi.org/10.1007/s00190-015-0867-4
Wu A (1996) Performance evaluation of the GPS Block IIR time keeping system. In: Proc 28th PTTI Meeting, pp 441–454
Zumberge J, Heflin M, Jefferson D, Watkins M, Webb F (1997) Precise point positioning for the efficient and robust analysis of GPS data from large networks. J Geophys Res: Solid Earth 102(B3):5005–5017. https://doi.org/10.1029/96JB03860

O. Montenbruck is an honorary professor at Technische Universität München (TUM) and former head of the GNSS Technology and Navigation Group at DLR's German Space Operations Center. His research interests comprise space-borne GNSS receiver technology, GNSS-based autonomous navigation systems, precise orbit determination, multi-constellation GNSS, and LEO PNT.

P. Steigenberger received his master and PhD degrees in Geodesy from Technische Universität München (TUM) in 2002 and 2009, respectively. Currently, he is a senior researcher at DLR's German Space Operations Center (GSOC) and chairs the IGS Multi-GNSS Pilot Project. His research interests focus on GNSS data analysis, in particular precise orbit and clock determination of GNSS satellites and the evolving navigation systems Galileo, BeiDou, and QZSS.